ROYAL SOCIETY OF CHEMISTRY

PAPER

Interannual, summer, and diel variability of CH$_4$ and CO$_2$ effluxes from Toolik Lake, Alaska, during the ice-free periods 2010–2015†

Werner Eugster, [ID] *[a] Tonya DelSontro, [ID] [b] Gaius R. Shaver [ID] [c] and George W. Kling [ID] [d]

Accelerated warming in the Arctic has led to concern regarding the amount of carbon emission potential from Arctic water bodies. Yet, aquatic carbon dioxide (CO$_2$) and methane (CH$_4$) flux measurements remain scarce, particularly at high resolution and over long periods of time. Effluxes of methane (CH$_4$) and carbon dioxide (CO$_2$) from Toolik Lake, a deep glacial lake in northern Alaska, were measured for the first time with the direct eddy covariance (EC) flux technique during six ice-free lake periods (2010–2015). CO$_2$ flux estimates from the lake (daily average efflux of 16.7 ± 5.3 mmol m^{-2} d^{-1}) were in good agreement with earlier estimates from 1975–1989 using different methods. CH$_4$ effluxes in 2010–2015 (averaging 0.13 ± 0.06 mmol m^{-2} d^{-1}) showed an interannual variation that was 4.1 times greater than median diel variations, but mean fluxes were almost one order of magnitude lower than earlier estimates obtained from single water samples in 1990 and 2011–2012. The overall global warming potential (GWP) of Toolik Lake is thus governed mostly by CO$_2$ effluxes, contributing 86–93% of the ice-free period GWP of 26–90 g CO$_{2,eq}$ m^{-2}. Diel variation in fluxes was also important, with up to a 2-fold (CH$_4$) to 4-fold (CO$_2$) difference between the highest nighttime and lowest daytime effluxes. Within the summer ice-free period, on average, CH$_4$ fluxes increased 2-fold during the first half of the summer, then remained almost constant, whereas CO$_2$ effluxes remained almost constant over the entire summer, ending with a linear increase during the last 1–2 weeks of measurements. Due to the cold bottom temperatures of this 26 m deep lake, and the absence of ebullition and episodic flux events, Toolik Lake and other deep glacial lakes are likely not hot spots for greenhouse gas emissions, but they still contribute to the overall GWP of the Arctic.

Environmental significance

Vast amounts of organic carbon are stored in Arctic permafrost soils. With climate warming it can be expected that an increasing amount of that carbon is freed as permafrost thaws, and can escape to the atmosphere *via* gas efflux from lakes. With the first continuous eddy covariance flux measurements over a deep Arctic lake in Alaska we provide evidence that during the ice-free period the effluxes of both CH$_4$ and CO$_2$ show pronounced diel and summer variations which are important, but no signs of episodic events with extremely high effluxes during the ice-free period could be found. This is in agreement with earlier estimates made for the Arctic and emphasizes the fact that deeper Arctic lakes are not the water bodies to be most concerned about regarding carbon emissions; however, better estimates of gas fluxes from the shallow lake-shore zones of such lakes are still needed.

1 Introduction

Arctic regions contain a vast reservoir of organic matter preserved in permafrost, the permanently frozen ground in northern high latitudes.[1] With climate warming, thawing of permafrost and the associated exposure of its organic matter to decomposition has become a great concern as a positive but unwanted feedback of the Arctic to climate change.[2–4] The role of open water bodies in the Arctic, which cover about 12–14 percent of the land surface area of the Alaskan North Slope[5,6] and up to 48% in some regions of Alaska,[7,8] has thus taken a prominent place in the estimate of greenhouse gas fluxes from Arctic ecosystems.[9] In this paper, we present eddy covariance (EC) flux measurements of the two primary greenhouse gases (CH$_4$ and CO$_2$) obtained during six ice-free lake periods (2010–2015). Because CH$_4$ effluxes have a climatic effect that is ≈34 times that of CO$_2$ effluxes[10] (on a 100 year time-scale, including

[a]Institute of Agricultural Sciences, Department of Environmental Systems Science, ETH Zürich, CH-8092 Zürich, Switzerland. E-mail: eugsterw@ethz.ch

[b]Department F.-A. Forel, Faculty of Science, University of Geneva, CH-1211 Geneva, Switzerland. E-mail: tdelsontro@gmail.com

[c]The Ecosystems Center, Marine Biological Laboratory, Woods Hole, MA, USA. E-mail: gshaver@mbl.edu

[d]University of Michigan, Ann Arbor, MI, USA. E-mail: gwk@umich.edu

† Electronic supplementary information (ESI) available. See DOI: 10.1039/d0em00125b

positive climatic feedbacks), our interest was in how continuous CH_4 flux measurements over Toolik Lake change previous estimates of Global Warming Potential (GWP) from Arctic lakes that were based only on CO_2 flux measurements (e.g., Eugster et al. 2003 (ref. 11)), but without an estimation of CH_4 effluxes.

Based on reports of huge amounts of CH_4 emitted from some Arctic water bodies,[12-16] expectations have become high that many or most Arctic lakes are or could be strong sources of CH_4, but also not everywhere.[17,18] With discrete sampling, e.g., bi-weekly surveys of CH_4 and CO_2 concentrations in lake surface waters or discrete short-term deployments of floating chambers to measure gas efflux at specific times, episodic events that could dominate daily or summer emissions would easily be missed or under sampled, particularly for CH_4.[19,20] Missing such events would lead to biased results and underestimates of emissions, but could be circumvented by using a higher resolution method, such as EC. For example, significant efflux events were observed during fall turnover[21] and after a substantial storm[22] in two Swiss lakes using EC. In addition to episodic events, strong diel patterns[20,23-26] could affect estimates of gas fluxes depending on when in the day samples were taken. Continuous monitoring techniques are essential for resolving such events. Furthermore, repeated measurements over several years at the same site, required for climatological studies, are limited in the Arctic.

Based on the first long-term EC flux measurements from a deep Arctic lake, this paper addresses the question: what cyclical processes and which episodic events are most relevant for obtaining a defensible ice-free period estimate of CH_4 and CO_2 effluxes from a deep Arctic lake? It also provides the foundation for follow-up investigations of the underlying mechanistic functional relationships between these fluxes and environmental drivers.

2 Experimental

2.1 Study site

Measurements were made on Toolik Lake ($68°37.830'$ N, $149°36.366'$ W, WGS84 datum) at 719 m asl, a relatively deep glacial lake (maximum depth $\approx$ 26 m) with a surface area of 1.5 km^2 located on the tundra north of the Alaskan Brooks Range. Instruments were mounted on a floating platform that was moored at approximately the same location every year $\approx$ 400 m from the nearest lake shore. Depth of the lake at this location was $\approx$ 12 m.

With the onset of snowmelt the ice on Toolik Lake begins to melt. Observations made in 2014 showed that the water arriving via overland flow and the main stream inlets initially flow over the thick ice sheet and gradually melt the ice from above along the shoreline, and then the flows move mainly under the ice and spread lakewide.[27] Once the ice sheet is sufficiently detached from the lake shores, stronger winds and associated waves can crack the ice, which then still covers most of the lake with floating chunks of ice that move around the lake as the wind shifts between the two predominant wind directions from the south and the north. The physical forces at work are too strong for eddy covariance instrumentation to be out on the lake. Therefore, the placement of equipment on the lake was only possible when the largest ice chunks on the lake were less than a few square-meters and few in number, typically between mid to late June (Table 1).

Similar to the early-season conditions, the float containing eddy covariance instrumentation had to be removed from the lake before any large ice areas had formed on the lake in the autumn. Ice-on after the ice-free period was defined as the time when ice first covered the entire lake until the following spring (i.e., temporary ice cover over night was not considered as the

Table 1 Summer flux totals observed at Toolik Lake during the ice-free periods 2010–2015

Year	2010	2011	2012	2013	2014	2015	Mean
Lake ice-off (thaw)[73]	Jun 14	Jun 16	Jun 17	Jun 28	Jun 24	Jun 10	Jun 18
Lake 100% ice covered (freeze)[73]	Oct 09	Oct 15	Oct 15	Oct 02	Oct 04	Sep 27	Oct 07
Ice-free days	117	121	120	96	102	109	111
Period with EC flux measurements on Toolik Lake							
EC to lake	Jun 22	Jun 14	Jun 21	Jun 29	Jun 28	Jun 20	Jun 23
EC from lake	Aug 18	Aug 20	Aug 22	Aug 17	Aug 22	Aug 21	Aug 20
EC days	55.9	64.7	60.6	48.6	54.9	61.4	57.7
EC coverage (%)	98.1	98.1	97.8	98.4	98.9	99.1	98.4
Half-hourly CH_4 flux records	2685	1724	2911	2333	2636	2441	
…acceptable quality (%)	84.6	50.4	94.2	90.6	90.5	63.2	78.9
…best quality (%)	58.6	33.6	67.2	62.6	66.7	46.3	55.8
CH_4 flux mean (mmol m^{-2} d^{-1})	0.119	0.063	0.201	0.130	0.093	0.147	0.126
CH_4 flux SD (mmol m^{-2} d^{-1})	0.074	0.058	0.075	0.049	0.038	0.070	0.061
Half-hourly CO_2 flux records	2644	1724	2908	2333	2586	2606	
…acceptable quality (%)	87	51.4	92.6	82.4	93.4	74.6	80.2
…best quality (%)	59.6	34.4	66.5	56.5	68.9	53.1	56.5
CO_2 flux mean (mmol m^{-2} d^{-1})	8.9	11.0	30.9	21.9	12.9	14.4	16.7
CO_2 flux SD (mmol m^{-2} d^{-1})	4.2	3.0	7.4	7.6	4.3	5.3	5.3
Estimated global warming potential (GWP) during ice-free period							
CH_4 flux sum (mg CH_4 m^{-2})	222.1	122.3	386.3	199.8	152.3	256.8	223.2
CO_2 flux sum (g CO_2 m^{-2})	46.0	58.4	163.5	92.3	57.8	67.7	81.0
Ice-free GWP (g $CO_{2,eq}$ m^{-2})	53.5	62.6	176.6	99.1	63.0	76.5	88.6

2182 | Environ. Sci.: Processes Impacts, 2020, **22**, 2181–2198

This journal is © The Royal Society of Chemistry 2020

first ice-on date). In this context it should be recalled that at this northern location the sun does not set from 23 May to 19 July, and thus "night" refers to the hours of day with lowest solar elevation angles. At the end of summers from 2010–2015, however, ice formation occurred later than observed in earlier years, and thus the platform was removed between 17 and 22 August for logistical reasons (Table 1).

2.2 Eddy covariance flux instrumentation

Flux measurements were made with a three-dimensional ultrasonic anemometer–thermometer (CSAT3, Campbell Scientific, Logan, UT, USA) in combination with a closed-path integrated off-axis cavity output spectrometer (ICOS) for CH_4 (FMA from Los Gatos Research, Inc., San Jose, CA, USA) and a nondispersive infra-red gas analyzer for CO_2 and H_2O (Li-7000, Li-Cor Inc., Lincoln, NE, USA). The CSAT-3 was mounted horizontally on a tripod (Met One Instruments, Inc., Grants Pass, OR, USA) screwed to the floating platform in such a way that measurement height above the lake surface was between 1.29 m and 1.62 m above the water surface. Two intake hoses were placed next to the CSAT-3 sensor head to guide air to the FMA and Li-7000 analyzers. A TriScroll 300 vacuum pump (Agilent, Santa Clara, CA, USA) was used to reduce the cell pressure of the FMA to the nominal 137 Torr (183 hPa). The Li-7000 did not require a vacuum in the sample cell, which allowed use of a KNF Neuberger N920 pump. A 500 m submersible AC power cable was used to provide the instruments and pumps on the float with mains power (120/240 V AC) from the power generator of Toolik Field Station (TFS). A step-up transformation of the voltage from 120 V AC to 600 V AC was necessary between lake shore and float to satisfy the high power demand of the vacuum pump.

The CH_4 flux measurements closely followed the technical set-up described in detail by Eugster and Plüss.[28] The CO_2 flux measurements used the same data collection concept. This data collection system consisted of an embedded Linux computer system (MOXA UC7408 Plus; Moxa Americas, Brea, CA, USA) to which the CSAT-3, FMA, and Li-7000 were connected *via* RS-232 serial communication connections. The continuous data stream from the CSAT-3 was recorded at 20 Hz and was used as the master to which the data streams from the FMA and the Li-7000 were merged in near real-time as described by Eugster and Plüss.[28] The system clock of the Linux computer was synchronized daily with internet network time domain servers, whenever the wireless link from the floating platform to TFS was active.

Instruments were not disturbed during the measurements unless maintenance, troubleshooting or additional sampling of surface waters were necessary. Ancillary meteorological data and data from sensors in the lake water were operated during the field seasons, but will be presented in a follow-up study where the response of fluxes to environmental drivers will be addressed in detail; the aim of the current paper is to assess the relevant timescales of variations that must be addressed in such a follow-up study.

2.3 Flux calculations

Flux calculations and quality control procedures closely followed the recommendations given by Vesala *et al.*[29] Our in-house eddy covariance flux software (eth-flux[30]) was adapted to the specific datasets obtained from Toolik Lake, but closely corresponds to standard procedures used for long-term flux measurements over land.[31–33] The same calculation method was used in an earlier study using similar equipment.[22]

In brief: calculations included (1) coordinate rotation of each 30 minute data segment to align the wind vector with the mean wind direction, thereby making (a) mean lateral wind speed $\bar{v} = 0$ m s^{-1} and (b) mean vertical wind speed $\bar{w} = 0$ m s^{-1}; (2) screening out unrealistic CO_2 mole fractions > 3000 ppm or < 330 ppm, or when the Li-7000 cell pressure was >1000 hPa or <500 hPa; (3) screening out unrealistic CH_4 mole fractions when the FMA sample cell pressure was >149.7 Torr or <122.0 Torr, or ringdown time was <16.5 ms; (3) determination of time lag between vertical wind speed and CH_4 and CO_2, respectively; (4) shifting the time series according to these lags within each 30 minute interval; (5) calculation of covariances; and (6) correction for density fluctuations caused my moisture flux (WPL correction;[34] details of the specific approach used here were given by Hiller *et al.*[35]).

Wave motion may affect the measurements obtained from an eddy covariance system. As investigated in detail by Eugster *et al.* (2003)[11] (see their Fig. 6), this mostly affects the variance of vertical wind speed with an increase on the order of 6%, but the effect is much small when reflected in the fluxes (or cospectrum[11]). Thus, no special flux correction to eliminate the traces of this oscillation was applied.[11]

The uncertainty of flux estimates was assessed based on statistical significance of covariances.[36–39] For data of best and good quality (flags 0 and 1 according to Foken *et al.*[33]), we obtained a median detection limit of 30 minute flux averages of ± 1.12 nmol CH_4 m^{-2} s^{-1} and 0.12 μmol CO_2 m^{-2} s^{-1}. This translates to uncertainties of ± 0.16 nmol CH_4 m^{-2} s^{-1} and 0.017 μmol CO_2 m^{-2} s^{-1} for daily median fluxes (average of 48 records), or better for median diel cycles at hourly resolution (average of up to 120 records per hour).

2.4 Gapfilling of missing flux data

To obtain daily and ice-free summer totals of fluxes, a procedure to fill data gaps is required. Here we only used measured and quality controlled data for the analysis, except for two special cases where gap filling was necessary: (i) the assessment of summer variations; and (ii) obtaining ice-free summer flux totals during the period of instrument deployment. The quality control procedure used here follows the flagging procedure suggested by Foken *et al.*[33,40] Both an integral turbulence test (ITC) and a steady-state test (SST) were performed using the 9-level flagging system, from which a general overall flux flag (range 1–9) was deduced according to Foken *et al.*[33,40] Table 1 gives the percentages of records that remained for the analysis. Acceptable quality refers to flags 1–8, and best quality refers to flags 1–6, whereas fluxes with flag 9 were not considered. Fluxes up to flag 8 were kept in the analysis to avoid potential erroneous removal of fluxes during ebullition events.[41]

Because no established procedure exists for filling flux data gaps in measurements carried out over a lake, we used the

median diel cycle approach for short gaps up to 1.5 days. For each 30 minute gap in the dataset the available measurements from the same hour of day measured up to 3 days before and after the date with the gap were considered to obtain the median flux for that hour of day in the period to fill the gap. In our dataset, 74–97% of the gaps observed in each summer season filled in this way were shorter than 3 hours, and 86–98% were shorter than 12 hours, except for 2011 (52% shorter than 3 hours). Compared to simple linear interpolation of short gaps, this procedure has the advantage that it is more robust when the longer-term flux signal is small compared to the variations from one available averaging interval to the next.

Gaps that were longer than 1.5 days were only filled for obtaining seasonal flux estimates using the daily average from the measured fraction of the respective season (see Section 4.5).

2.5 Lake surface temperature and stability measurements

Lake surface temperatures T_s (°C) were measured with a down-looking CG3 pyrgeometer (Kipp & Zonen, Delft, the Netherlands) of a four-way CNR1 net-radiometer using Stefan–Boltzmann's law,[42]

$$T_s = \sqrt[4]{\frac{LW_\uparrow}{\sigma\varepsilon}} - 273.15, \tag{1}$$

with $LW_\uparrow$ measured absolute outgoing long-wave radiation, σ the Stefan–Boltzmann constant (5.67×10^{-8} W m^{-2} K^{-4}), and an emissivity $\varepsilon = 0.98$ for water.[43]

The Monin–Obukhov[44] stability parameter z/L was determined from EC flux measurements as

$$z/L = -\frac{z\kappa\overline{w'T_v'}}{u_*^3 \frac{T_v}{g}}, \tag{2}$$

with z measurement height above lake surface (m; see Section 2.2), κ the von Kármán constant (0.40, dimensionless), $\overline{w'T_v'}$ buoyancy flux (K m s^{-1}), u_* the friction velocity (m s^{-1}), T_v virtual (sonic) temperature (K), and g the gravitational acceleration (9.81 m s^{-2}).

2.6 Statistical analyses

All statistical analyses were done with the open-source statistical software R version 3.6.1.[45] Both CH_4 and CO_2 fluxes measured over lakes tend to show a variability of 30 minute average fluxes that is much larger than the longer-term mean flux itself. Hence, we mostly use robust statistics (median, quantiles, inter-quartile range) in our analysis. For comparability with other published values we also report arithmetic means and standard deviations, which are commonly used when sampling discretely with floating chambers.

Spline smoothing was done with a local polynomial regression fitting (loess function in R); the span parameter for smoothing set to 0.5 when smoothing diel cycles of data, and to 0.25 when smoothing ice-free period data.

2.6.1 Wavelet analysis. Morlet wavelet periodograms were calculated using the dplR package version 1.7.0 in R. Wavelet decomposition can be considered as a special kind of frequency

analysis similar to the Fourier transformation, but with the difference that a Fourier transform analysis assumes that the time series under investigation is stationary and periodicity is constant over the time period of measurements. Contrastingly, a wavelet analysis also can resolve segments in a time series with higher or lower amplitude of a given periodicity or frequency, as it is normally required, for example, in seismic or dendrochronological analyses. Similar to episodic events in earthquake research, fluxes measured over a lake may be primarily governed by ebullition or lake turnover (mixing) events (see e.g., Schubert et al.[21]), which would be more easily identified with a wavelet analysis. Our approach closely follows standard procedures explained by Nason[46] using gapfilled data. The term "Morlet wavelet" refers to the original work that is the foundation of the analysis.[47]

For a quantitative assessment of the relevance of diel and weekly cycles we proceeded as follows: the five wavelets with periods centered with the diel or weekly cycle were used to determine the fraction of measurements with a statistically significant cyclicity (i.e., the wavelet power > the significance threshold determined by the wavelet analysis). The five wavelets used for this assessment have a bandwidth of 20 to 27 hours for the diel cycle, and 5.9 to 7.8 days for the weekly cycles that we report for each summer season.

2.6.2 Flux footprint analysis. We oriented the instruments to have the maximum fetch, undisturbed by the float and tower itself, in the direction of the most common winds (Fig. 1). The overall flux footprint area for each summer was then calculated using the Kljun footprint model[48,49] using the 2-d integrated footprint for each 30 minute flux average, which was then aggregated for the seasonal maps. In all summers the typical extent of the footprint area was constrained to 100–150 m around the tower (Fig. 2) with slightly larger areas in later years with a higher measurement height than in the earlier years with lower measurement heights. In all summers the dimension of the footprint was small enough to be entirely within the lake
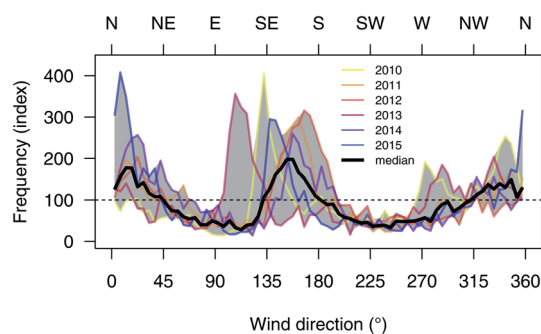

Fig. 1 Wind direction frequencies during ice-off periods 2010–2015 at Toolik Lake. The frequency index 100 indicates the expectation value of a uniform distribution of wind directions. The gray band shows the range of all six years, the bold line is the median from all years. Note that the measurement platform mooring was not rigid, and thus the shift in peak wind directions in the E–S sector rather reflects the differences in configuration of the platform mooring during individual summers, and most likely is not indicating a real difference in wind directions.

2184 | Environ. Sci.: Processes Impacts, 2020, **22**, 2181–2198

This journal is © The Royal Society of Chemistry 2020

water surface (Fig. 2), given the distance to the nearest shoreline of ≈ 400 m and a lake area of 1.5 km^2 (see Section 2.1).

It is well known that CH_4 and CO_2 concentrations are not constant in the surface waters of a lake.[50] Manual sampling of surface water CH_4 and CO_2 pressures in all summer seasons 2010–2015 showed a clear supersaturation of both gases with respect to the atmosphere (G. W. Kling, pers. comm.). This supersaturation might be somewhat stronger over shallower parts of the lake, and thus these measurements might underestimate the supersaturation for the entire lake. However, because of our analysis of the eddy flux footprint (see Fig. 2) we assume that our flux measurements are representative for the part of Toolik Lake that is deeper than 2 m (>85% of Toolike Lake; Fig. 2).

2.7 Sonar surveys to detect ebullition

In 2012 an extensive sonar survey was carried out in a similar way as was done by DelSontro et al.[51] before using a 120 kHz (7° beam angle) split-beam scientific echosounder (Simrad EK60, Kongsberg Maritime, Norway), operating at 5 Hz. Surveys were carried out on 19, 23, and 24 July 2012, covering a total footprint area of 8100, 15 800, and 11 000 m^2, respectively, of Toolik Lake. The average lake depth covered during the three campaigns was 11, 7, and 8.5 m. The total track length was 34.5 km in a regular pattern, providing a representative snapshot sample of the lake (see ESI†).

2.8 Influences of instrumental failures on periodicities

A nearby lightning strike put the electronics of the serial port of the LGR FMA out of order on 2 July 2015, such that a temporary fix was necessary to continue with measurements at this remote

Fig. 2 Flux footprints for each ice-free period 2010–2015. The footprint of 2015 is also placed at correct scale on the bathymetric map of Toolik Lake. The outer bold lines indicate the extent of the 90% flux footprint area of the entire summer. The bold line in the hashed area (25–75% footprint area) of each footprint is the median distance from the EC measurements (in the center of each footprint). Circles show equal distances from the EC instruments at 10, 30, 50, 70, and 90 m. Toolik Lake bathymetric map by Toolik Field Station GIS.

site where sending the instrument to the manufacturer for repair would have meant the end of measurements for that last year of the project. The temporary fix was done by activating the second, unused serial port on the LGR FMA computer mother board, solder the wires to its open connectors, and then reroute the Linux device name (/dev/ttyS0) to that second port. The CSAT-3 also reported three error conditions: (1) unacceptably high differences in speed of sound measurements among the three measurement axes; (2) poor signal lock; and (3) too low amplitude of sonic signal. However after hard power reset the CSAT-3 operated normally. The follow-up outages of data transfer from the FMA to the Linux data acquisition system thus were related to that defect on the instrument from the first thunderstorm with lightning. Because we use fully digital data acquisition,[28] we could ascertain that the data that actually could be collected are of good quality and are not affected by the damage observed on the serial port of the FMA.

The CO_2 instrumentation was not affected in the same way by the same lightning strike near the float. However, the Li-7000 was sensitive to the motions of the float. The instrument uses a phase-lock-loop system for the filter disk that has the three filters for CO_2, H_2O, and reference (neutral for both CO_2 and H_2O). This filter disk had too low inertia to provide perfect phase lock when float motions were increased. Because these conditions are well documented in the housekeeping variable of the Li-7000 (diagnostic flags), it was possible to screen out all CO_2 raw data values where the phase-lock-loop flag indicated an issue. Hence, the true sampling frequency from the Li-7000 was reduced to slightly below 20 Hz under conditions with phase-lock-loop problems.

Testing in the laboratory at Toolik Field Station in 2010 confirmed that no such issues occur when the same instrument is placed on a sturdy laboratory bench after it had indicated an increased number of occurrences of phase-lock-loop issues. We thus deduced from this test that optical instruments with moving parts require additional attention and data treatment for reliable eddy covariance flux measurements on a moving platform. In reality, reducing the sampling rate below the nominal 20 Hz is no problem, and depending on measurement height above surface, even lower sampling frequencies can still produce flux measurements with acceptable quality.[28,52]

3 Results

3.1 Periodicities in CH_4 and CO_2 fluxes of Toolik Lake

Eddy covariance greenhouse gas fluxes from Toolik Lake tend to show a large temporal variability that is partly related to the measurement technique employing fast response sensors, but also to cyclical processes related to diel or longer-term variations in environmental conditions in the atmosphere above and the water below the lake surface. Wavelet decomposition thus is a powerful method to find periodic patterns in time series. Fig. 3 shows the CH_4 flux Morlet wavelet periodogram for each ice-free open-lake season, and Fig. 4 shows the same for the CO_2 flux. Each panel shows the time series of eddy covariance flux measurements with day of year on the x-axis, and the Morlet wavelet periodogram below. The number of periods in the total time series of each season is shown with the y-axis on the left,
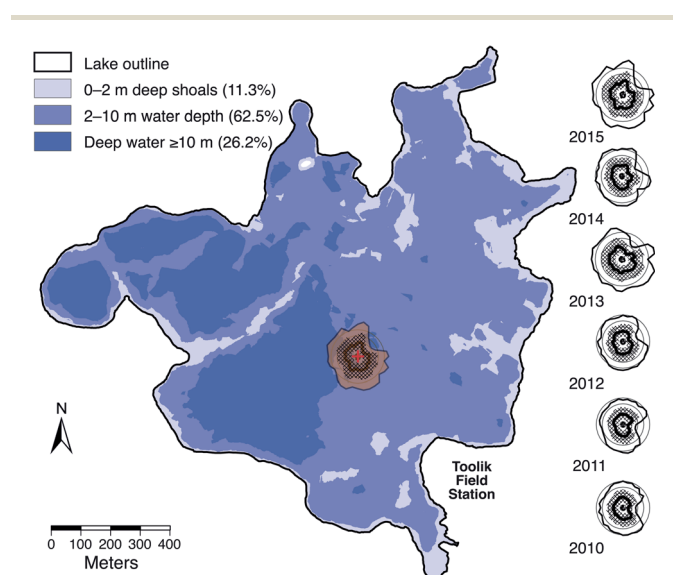
This journal is © The Royal Society of Chemistry 2020

Environ. Sci.: Processes Impacts, 2020, **22**, 2181–2198 | **2185**

and the corresponding cycle length in number of days is shown with the y-axis on the right. Horizontal white dashed lines show the diel and weekly cycles for reference. Only red areas with bold boundaries are statistically significant at the 95% significance level or better (corresponding to $p < 0.05$).

During all summers the diel cycle is often—but not always—pronounced over several days and significantly different from random variations. In years 2012, 2013, and 2014 the diel cycle in CH_4 fluxes was more persistent in the second half of the ice-free period than in the first half. Contrastingly, years 2010 and 2015 have periods of several days with persistent diel cycles, which were interrupted by periods without diel cycles. In the

special case of year 2015, several instrument failures in the CH_4 flux measurements (hashed areas in Fig. 3) make interpretation more difficult (see Section 2.8), but these failures were always related to thunderstorms at the end of fair weather periods; thus, it is not unlikely that the significant diel cyclicity was restricted to the periods covered with data. CO_2 fluxes were less affected by these storms than CH_4, but the CO_2 fluxes do not show a substantially different pattern in 2015 than the CH_4 fluxes.

In the case of CO_2 fluxes (Fig. 4) the diel cycles are even more pronounced than those of CH_4 fluxes (Fig. 3). The fraction of the measurements with a significant diel cycle is always higher in
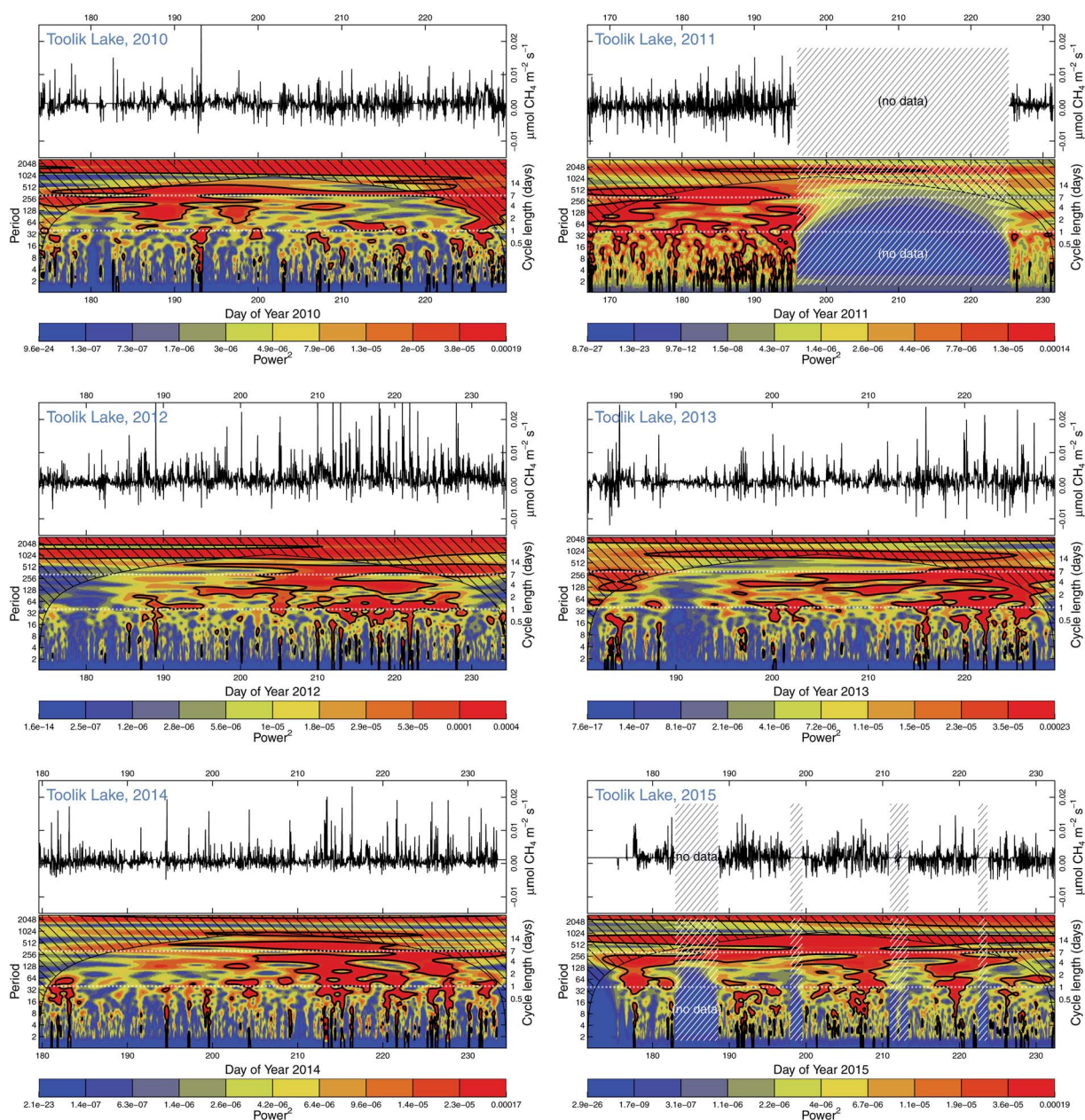

Fig. 3 Morlet wavelet periodograms of CH_4 fluxes during the ice-free periods 2010–2015. The time series of 30 minute fluxes are shown in the top part of each panel, and the Morlet wavelet decomposition below it. The black hashed areas are affected by the boundary conditions of the transformation and should be ignored. White hashed areas show major data gaps. Solid contours show features significant at the 95% level ($p < 0.05$). Horizontal white dashed lines show daily and weekly cycle lengths (right axis).
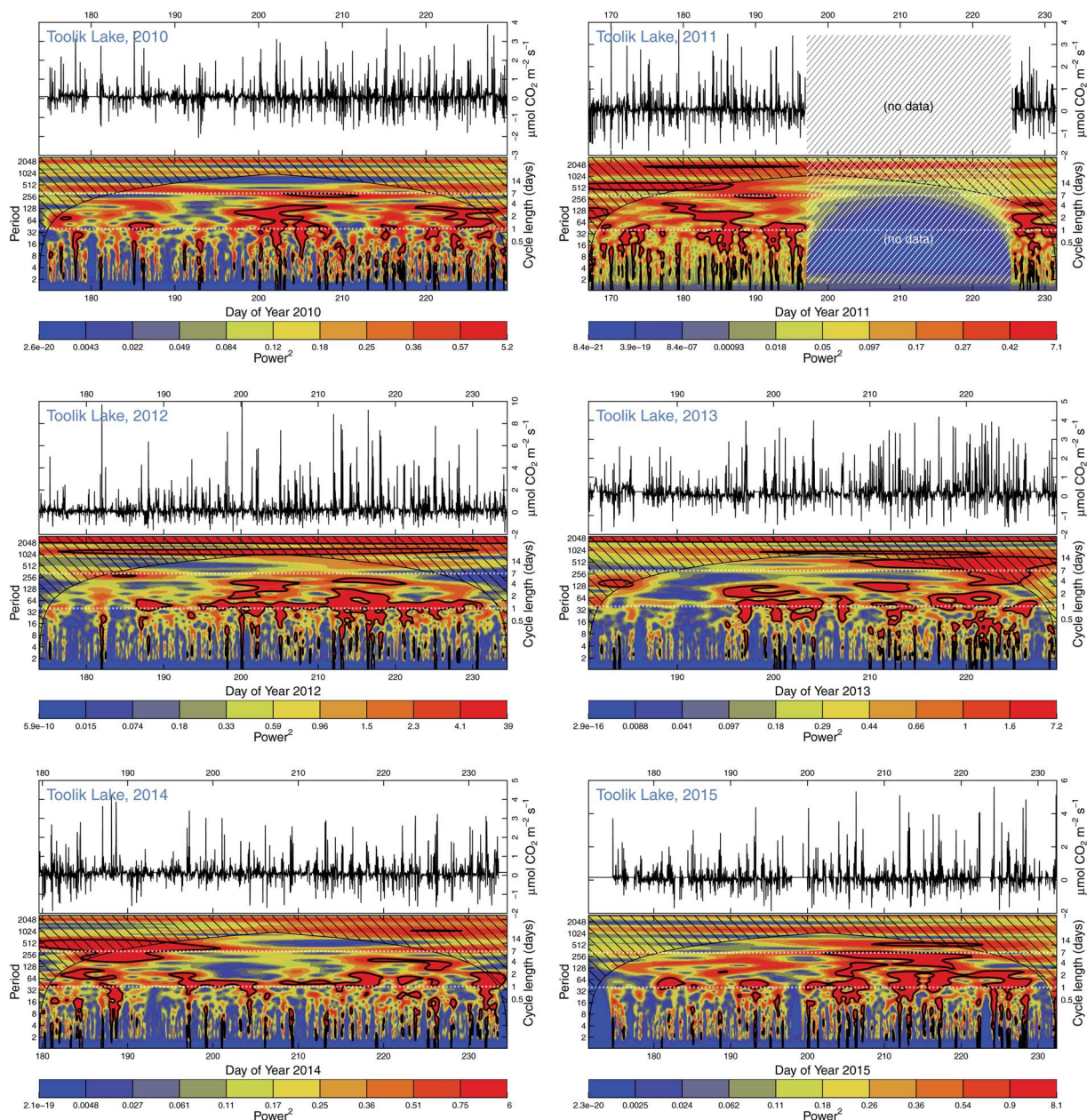
2186 | Environ. Sci.: Processes Impacts, 2020, 22, 2181–2198

This journal is © The Royal Society of Chemistry 2020

Fig. 4 Same as in Fig. 3, but for CO_2 fluxes.

a pairwise comparison of years (Fig. 5). Contrastingly, cycles on the order of the weekly cycle were clearly more pronounced in the CH_4 fluxes than CO_2 fluxes in all years. Given the short ice-free period of Toolik Lake that typically only lasts for 1.5–2.5 months, these multi-week cycles are a major portion of the ice-free summer period; therefore, we focus on the diel and ice-free summer cycles of gas effluxes from the lake.

3.2 Diel cycles of CH_4 and CO_2 effluxes

The diel cycles of both CH_4 (Fig. 6) and CO_2 (Fig. 7) were pronounced in all years, with 2015 being an exception in case of CH_4 fluxes (Fig. 6f). The diel peak of the hourly median flux (circles in Fig. 6 and 7) of CH_4 typically occurred between 2 and

6 hours in the morning (Alaska Daylight Time, AKDT) and 2 to 5 hours AKDT in case of CO_2 efflux; thus the peak fluxes are synchronous with the lowest solar angle (around 2 hours AKDT) or the first hour after local solar minimum. Recall that the sun does not set at this northern location in the months of June and July, and only shortly disappears below the horizon in August.

The highest daytime hourly median CH_4 effluxes tend to be around 50% of nighttime fluxes (down to 20% in 2014; Fig. 6e), but only around 20% in the case of CO_2 effluxes (Fig. 7). The day-to-day variability, however, is substantial for both gases, as is indicated by the color bands showing the inter-quartile range for each hour of day in Fig. 6 and 7. While this day-to-day
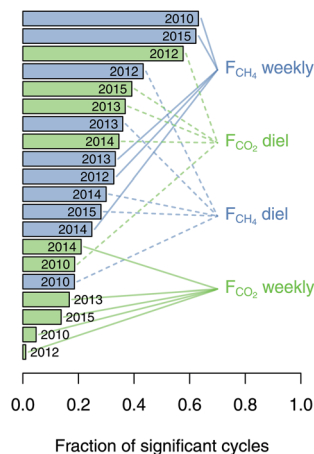
Fig. 5 Fraction of the time period covered in each year shown in Fig. 3 and 4 during which the diel or weekly cycle of the CH_4 and CO_2 fluxes were significant at $p < 0.05$.

variability within each hour of day only shows a weak relationship with the absolute CH_4 flux magnitude, this is not the case for CO_2 fluxes, where nocturnal variability is clearly higher than daytime variability (Fig. 7).

3.3 Ice-free summer periodicities of CH_4 and CO_2 effluxes

The ice-free summer periodicities of both CH_4 and CO_2 fluxes show a similar periodicity with timescales of about a week or longer (Fig. 8 and 9; the spacing between date labels is two weeks), which is in agreement with the Morlet wavelet periodograms (Fig. 3 and 4). There is, however, no consistent trend across all years. Only in the case of CO_2 fluxes did the within-day variability (illustrated by the shading around each median flux) increase during some years (2012, 2013, Fig. 9c and d), but not so much in other years (2014, 2015, Fig. 9e and f).

Daily median CH_4 effluxes started with low magnitudes at the beginning of the summer season in 2010 and ended with the highest efflux when the equipment had to be removed from the lake (Fig. 8a). Contrastingly, in 2015 the daily median CH_4 efflux started at a high level of around 2 nmol m^{-2} s^{-1} at the beginning of the ice-free period but ended almost neutral (Fig. 8f). In 2014, CH_4 effluxes were generally low with a slight increase towards the end of the ice-free period (Fig. 8e).

When all available flux measurements from all six summers 2010–2015 are combined (Fig. 10), the median diel cycle shows a 2-fold and a 4-fold difference between nighttime high and daytime low fluxes for CH_4 and CO_2, respectively. Contrastingly, the median summer cycle shows an increasing trend of CH_4 fluxes in the first half of the ice-free period followed by almost constant daily median fluxes (Fig. 10b). A reversed pattern was observed in CO_2 fluxes with daily median fluxes being almost constant until the last week of the ice-free period when instruments were operated on the lake (Fig. 10d), during which an upward trend can be seen. In both cases, the early-season to late-season differences remained within a 2-fold range, similar to the diel cycle observed in CH_4 fluxes, but clearly less pronounced than the observed diel cycle in CO_2 fluxes. Also

important to note is that median fluxes for both gases at all scales were positive, indicating a persistent efflux from the lake over the ice-free period.

3.4 Ice-free mean fluxes and interannual variations

For reference with earlier literature based on discrete chamber flux measurements from Toolik Lake, the daily aggregated fluxes shown in Fig. 8 and 9 were averaged to daily means for each year (Fig. 11). Although robust statistics (using medians and quantiles) is helpful for interpreting noisy data such as eddy covariance flux estimates, most existing studies assume that such variations are normally distributed around a mean value and thus report arithmetic mean and standard deviation. In Fig. 11 the bar size corresponds to the arithmetic mean, and whiskers show ±1 SD. For comparison with the data presented in Fig. 8 and 9, the ice-free summer interquartile ranges and median fluxes were added with a darker or brighter colored box and a white circle, respectively.

While variability during the ice-free period was quite comparable among years in both CH_4 and CO_2 fluxes (Fig. 11a and b), considerable interannual variation was found, with a 3 to 4-fold difference between the year with the highest and lowest fluxes of both CH_4 and CO_2. Yearly magnitude trends between CO_2 and CH_4 did not match, except for the fact that maximum emissions occurred in 2012 for both gases. The mismatch in overall trend thus indicates that CH_4 and CO_2 fluxes were governed by different physical and chemical processes. In addition, all fluxes observed over Toolik Lake were likely diffusive, as no ebullition was detected during a sonar field campaign to detect bubbles that occurred in July 2012 (see ESI†) when CH_4 concentrations were highest (Fig. 10b and 11a). Only a few features recorded during one of the three July 2012 sonar campaigns could potentially be bubble plumes, but the results are not conclusive (see ESI†). The features were not associated with any single bubble tracks, which is typically the case.[51,53] Because no single bubble tracks were observed, we could not make any estimations on the potential flux from these features if they were indeed plumes.

When converting both trace gas fluxes to global warming potentials (GWP) in units of g $CO_{2,eq}$ m^{-2} on a 100 year timescale (Fig. 11c and Table 1), it becomes clear that it is primarily the CO_2 efflux from Toolik Lake that dominates the GWP, contributing 86–93% to the lake's GWP.

Plotting cumulative fluxes for both trace gases over the ice-free periods requires some interpolation of the larger data gaps. Fig. 12 shows that years with almost complete data coverage show no signs of special singular events, such as deep mixing from storms that might lead to short-term emission peaks. The changes in slope of each cumulative curve indicate the ice-free emission cycle with minor modifications due to diel fluctuations. In relation to the variation of median diel fluxes the interannual variations were a factor 4.1 and 1.8 larger for CH_4 and CO_2 fluxes, respectively. Hence, using the yearly averages presented in Fig. 11a and b for interpolating longer data gaps (shown with thin dashed lines in Fig. 12) can be considered a valid approach to obtain ice-free totals for each year.
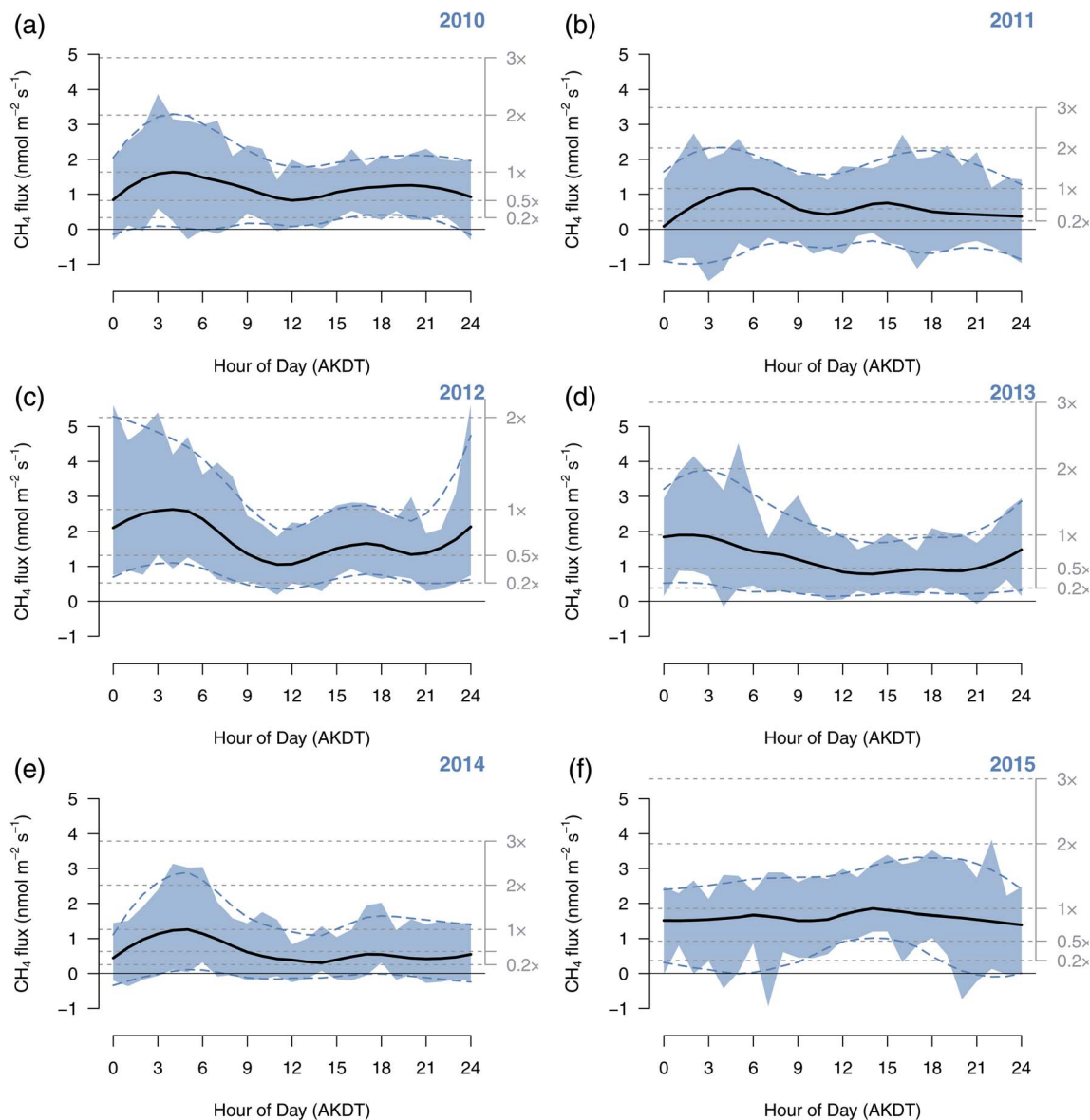
2188 | *Environ. Sci.: Processes Impacts*, 2020, **22**, 2181–2198

This journal is © The Royal Society of Chemistry 2020

Fig. 6 Median diel cycles of CH_4 flux during each ice-free period 2010–2015 (a–f). Circles show the median flux for each hour of day. The blue area is the inter-quartile range (25–75% confidence interval for each hour of day). The black solid and blue dashed lines are smoothed fits to the medians and the boundaries of the inter-quartile range, respectively. Gray dotted lines show the levels of relative fluxes where 1× is defined by the maximum of the black solid spline fit to the hourly medians.

4 Discussion

These are the first eddy covariance flux measurements from multiple ice-free summers of a deep lake in the low Arctic. They are a follow-up to the pioneering EC measurements made over Toolik Lake in years 1994 and 1995,[11] which only quantified short-term CO_2 fluxes and not CH_4 emissions.

4.1 Short-term periodicities in CH_4 and CO_2 fluxes

As described in Section 2.8, instrument failures and wave motion did not contribute to periodicities in the EC flux data. Both CH_4 and CO_2 showed significant periodicities at shorter time scales than the diel timescale as seen in Fig. 3 and 4,

namely in the lowest part of the Morlet periodograms with periods <8 that correspond to cycle lengths of <4 hours at 30 minute resolution. We consider these periods to be related to the artefact that eddy covariance flux measurements are typically averaged over fixed clock-based intervals of 30 minutes. In reality, eddies of any size do not respect these artificial boundaries between averaging time intervals, and thus often a strong deviation in one direction is counterbalanced at least in part by a deviation in the other direction in the following averaging interval. Such variations are not noise and not random variations, hence they are correctly identified as significant variations, but they basically indicate that depending on atmospheric conditions the turbulent time scale in the atmosphere is on the order of 1 h during daytime to 4 h during
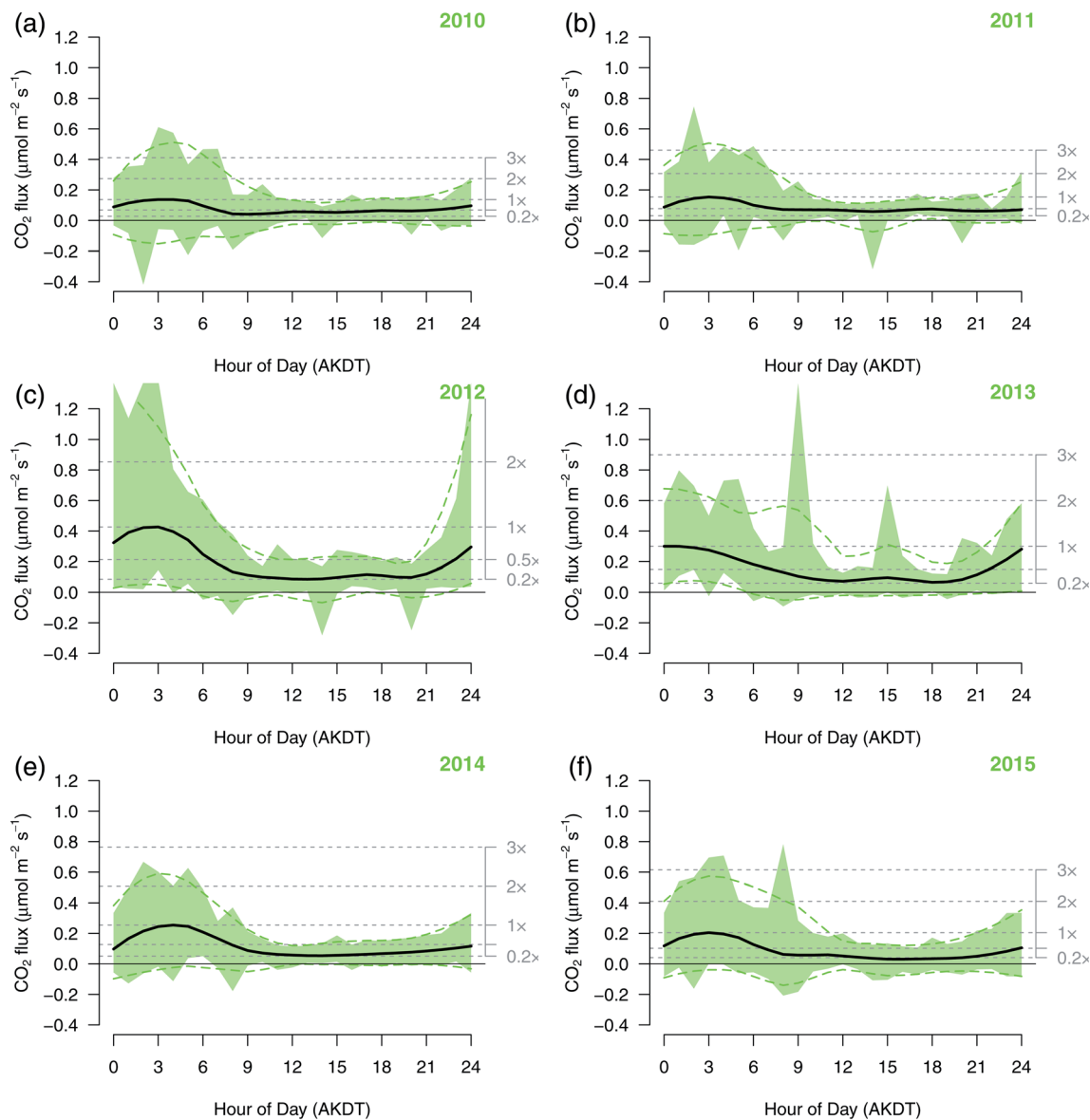
This journal is © The Royal Society of Chemistry 2020

Environ. Sci.: Processes Impacts, 2020, **22**, 2181–2198 | **2189**

Fig. 7   Same as in Fig. 6, but for CO_2 flux.

the night. This problem is well known from EC flux measurements above tall canopies.[54,55] This is also the reason why individual 30 minute periods of EC measurement can show a flux < 0 μmol m^{-2} s^{-1} due to such artefacts. For example, Fig. 6b shows a relevant share of negative CH_4 fluxes in 2011, although on average CH_4 evades from the water body to the atmosphere.

4.2   Diel cycles of CH_4 and CO_2 fluxes

In contrast to land surfaces, a lake surface is warmer than the atmosphere at night during the ice-free period, and thus convective conditions dominate at night but much less so during the day (Fig. 13b) when the lake surface often is colder than the atmosphere above.[29] Thus, in contrast to EC flux measurements over land, there is rarely an issue with stagnant air and stable stratification of the atmosphere at night.[29]

Therefore, nocturnal EC flux measurements can be considered at least as reliable as daytime measurements when measurement instruments are placed on the lake such that the measurement footprint lies entirely over the lake surface and influence from land is minimal.

Peak effluxes of CH_4 (Fig. 6) and CO_2 (Fig. 7) tended to occur during the night in most years. Night in this context means the period with low solar elevation angle, but it does not mean that it was very dark. The diel cycles of CO_2 fluxes, which have also been observed elsewhere,[56,57] are in agreement with the interpretation presented in Eugster *et al.* (2003)[11] that the enhanced nocturnal CO_2 effluxes may at least in part be related to the mixing of CO_2-rich waters from the deeper layers to the lake surface, although a decrease in photosynthetic uptake at night may also be important. The enhancement of nocturnal CO_2 effluxes is most prominently seen in the 2012 ice-free period
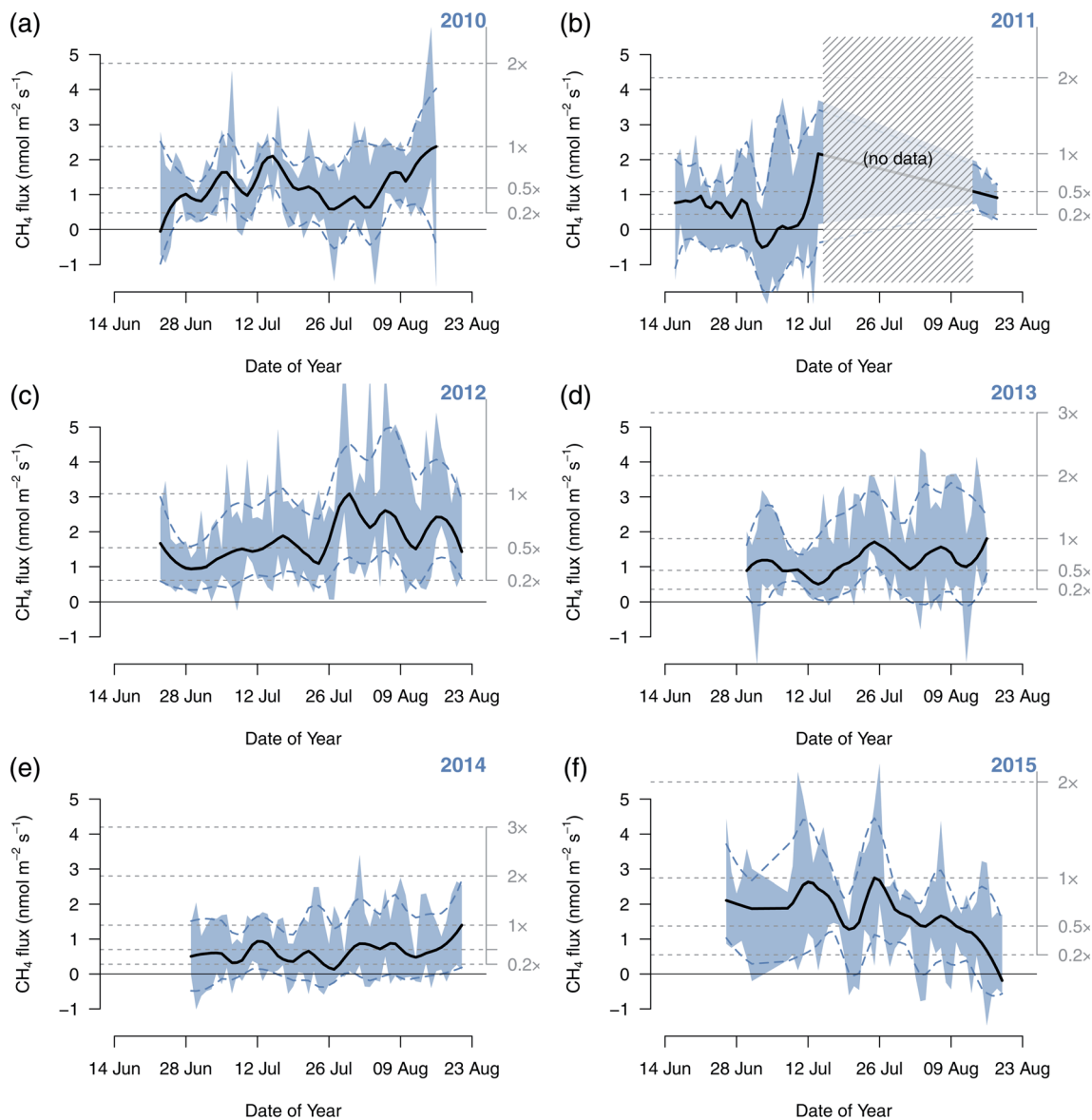
Fig. 8 Median ice-free summer cycle of CH_4 flux during each ice-free period 2010–2015 (a–f). Circles show the median flux for each hour of day. The blue area is the inter-quartile range (25–75% confidence interval for each hour of day). The black solid and blue dashed lines are smoothed fits to the medians and the boundaries of the inter-quartile range, respectively. Gray dotted lines show the levels of relative fluxes where 1× is defined by the maximum of the black solid spline fit to the hourly medians.

(Fig. 7c), but occurs in most years. A diel cycle of CO_2 flux with nocturnal flux peaks was also observed in a long-term study from Lake Valkea-Kotinen, a boreal lake in southern Finland,[58] but contrasts with observations from another boreal lake in Finland, where EC measurements did not show a diel cycle in CO_2 flux, but only in the CH_4 fluxes.[25]

A diel cycle of CH_4 fluxes is also seen at Toolik Lake, but it was clearly less pronounced than that of CO_2, even in 2012 (Fig. 6c) with the highest median and peak CH_4 effluxes of all six ice-free periods investigated. The daily range of median fluxes is typically on the order of 2× for CH_4 fluxes (Fig. 6) but on the order of 4× for CO_2 fluxes (Fig. 7). The timing of the peak effluxes coincides with the hours of day when the surface cooling of the water is strongest and promotes convection[59] (Fig. 13). The relative

contributions of both processes will need an in-depth assessment that would go beyond the scope of this paper.

The evidence of a pronounced diel cycle of CH_4 and CO_2 effluxes (summarized for all summers in Fig. 10a and c) indicates that when discrete sampling with other techniques is done over such lakes, careful considerations about time of day when measurements are taken are required; for example, if sampling is always done during the day then efflux estimates may be conservative (i.e., Kling et al.[5,60]). Alternatively, measurements carried out at a consistent time of day would allow to scale up to daily values. This approach is complicated by the fact that not all summers showed pronounced diel cycles as were observed in 2012; e.g., the diel cycle of CH_4 fluxes was almost nonexistent in 2015. In contrast, the diel cycle of CO_2 fluxes showed similar
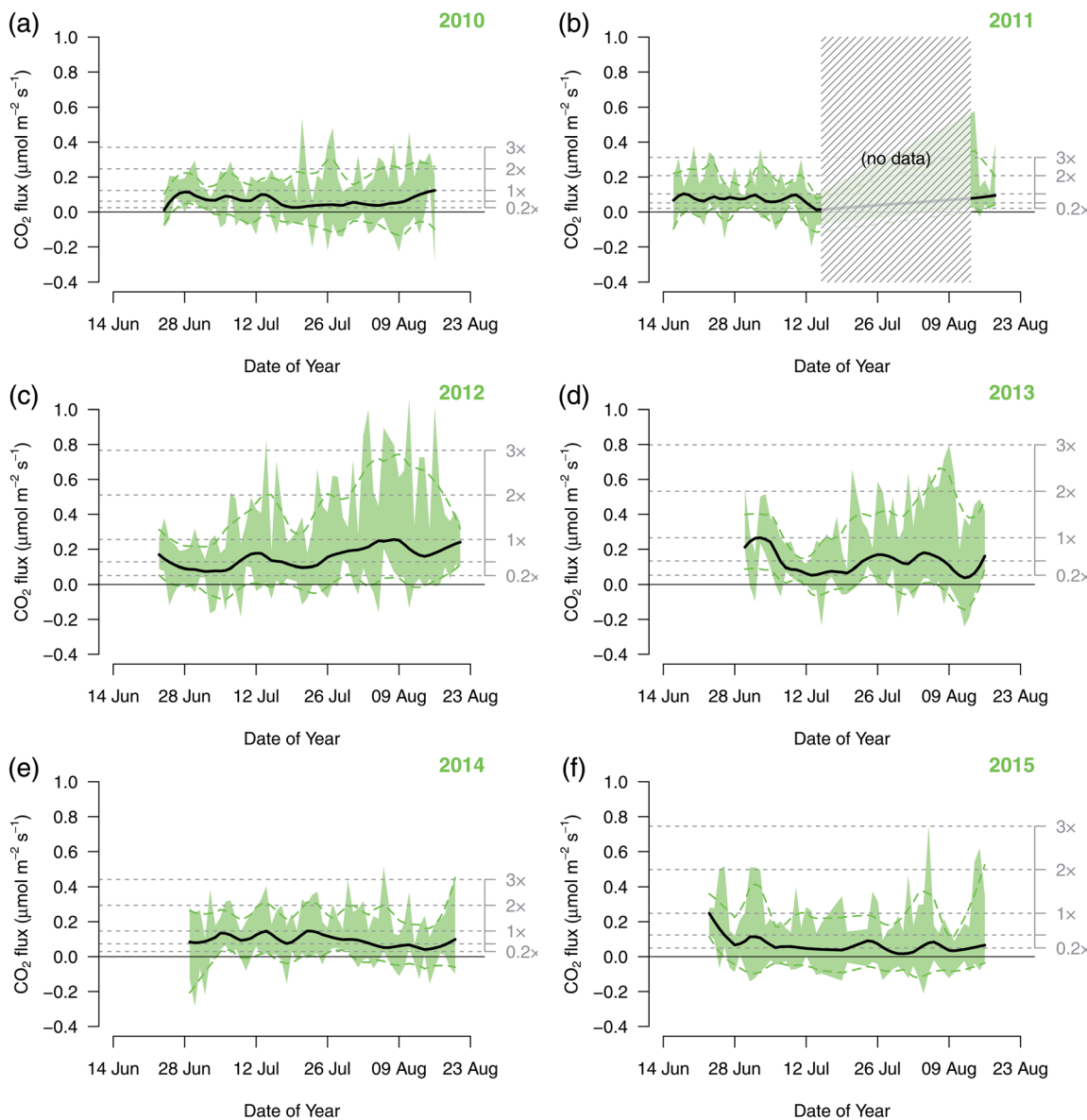
This journal is © The Royal Society of Chemistry 2020

Environ. Sci.: Processes Impacts, 2020, **22**, 2181–2198 | **2191**

Fig. 9 Same as in Fig. 8, but for CO_2 flux.

ratios of the maximum *vs.* minimum median fluxes (indicated by the factor given on the right-hand axis in Fig. 7), but with year-specific absolute amplitudes.

4.3 Ice-free summer periodicities of CH_4 and CO_2 effluxes

While the diel cycles of both CH_4 and CO_2 effluxes showed a relatively clear and simple pattern, the yearly ice-free cycles observed are more difficult to generalize. The years with almost complete data coverage (2010, 2012–2015; Fig. 8 and 9) as well as the Morlet periodograms (Fig. 3 and 4) indicate that the entire ice-free fluxes for each year can be estimated well even if there are breaks in the continuous EC measurements. In other words, the variation over the ice-free period is low enough that weekly sampling that accounted for the diel cycles could provide a defensible ice-free summer flux estimate.

Based on our direct flux measurements we estimated that 86–93% of the lake's GWP is due to CO_2 fluxes, thus only 7–14%

originating from CH_4. A recent study by Sepulveda-Jauregui *et al.*[61] estimated that roughly 65% of typical non-yedoma lakes' GWP stems from CH_4 fluxes. This discrepancy indicates that future studies should address why direct flux measurements (*via* EC) differ so strongly from flux calculations (*i.e.*, piston velocity modeling) based on discrete sampling, which may have better spatial coverage but always a lower temporal resolution than EC flux measurements.

4.4 Estimating fluxes from summer measurements

In general, ebullition could be a significant emission pathway during ice-melt or freeze-up considering bubbles have been observed in iced-over lakes of the north.[62] A previous study of 40 Alaskan lakes[61] reported an ebullition estimate for Toolik Lake based on ice surveys, but no other specifics on location or degree of ebullition was given. We, on the other hand, did not observe any ebullition *via* our 2012 sonar survey in Toolik and
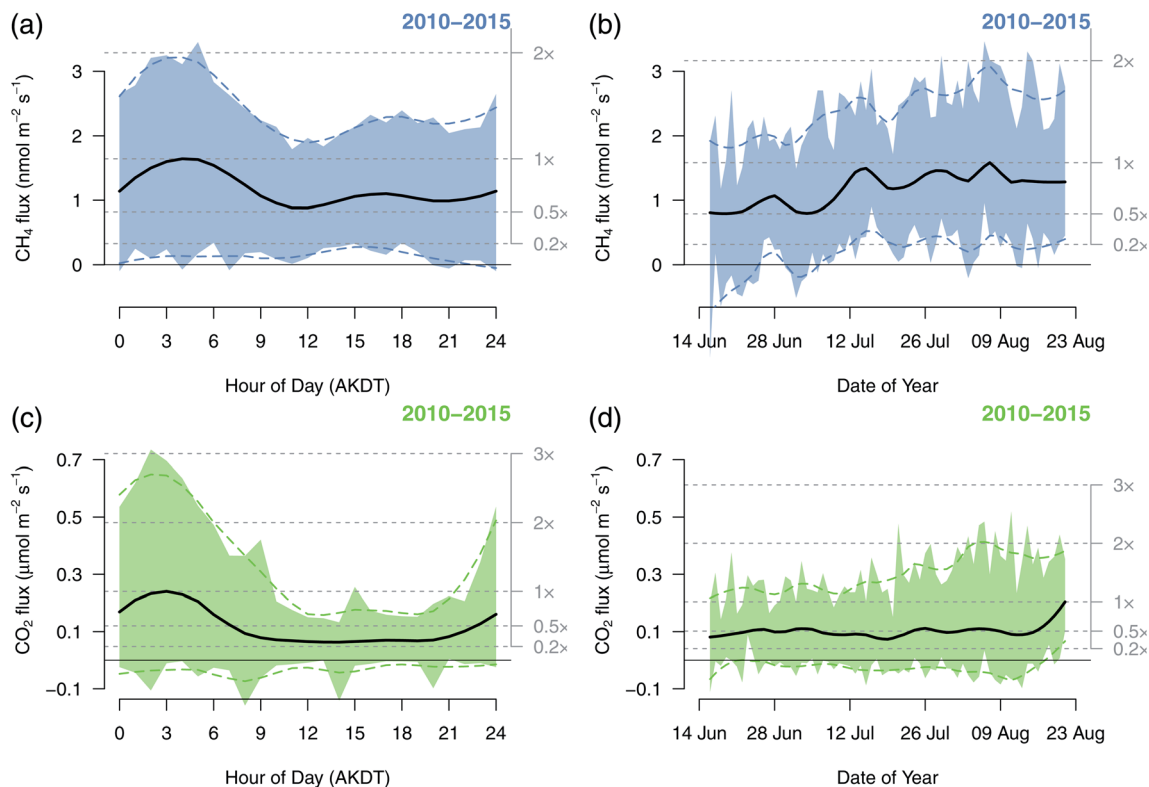
Fig. 10 Median diel (left; a and c) and ice-free summer (right; b and d) cycles combined with all data from all summers 2010–2015. For the seasonal cycles only days with full data coverage were considered. Circles show the median flux for each hour of day (left) or day of year (right). The blue and green areas are the inter-quartile range (25–75% confidence interval for each hour of day or day of year). The black solid and colored dashed lines are smoothed fits to the medians and the boundaries of the inter-quartile range, respectively. Gray dotted lines show the levels of relative fluxes where 1× is defined by the maximum of the black solid spline fit to the hourly or daily medians.

have no evidence that ebullition is a significant CH_4 emission pathway in this lake, even during ice-melt or freeze-up (T. Del-Sontro, pers. comm.). Ebullition is typically most prevalent during the warmest part of the summer as production rates are temperature-dependent and emissions scale with temperature.[63] Lake depth and sediment temperature of Toolik are however not independent variables due to the presence of permafrost that helps keep lake bottom temperatures below 5–
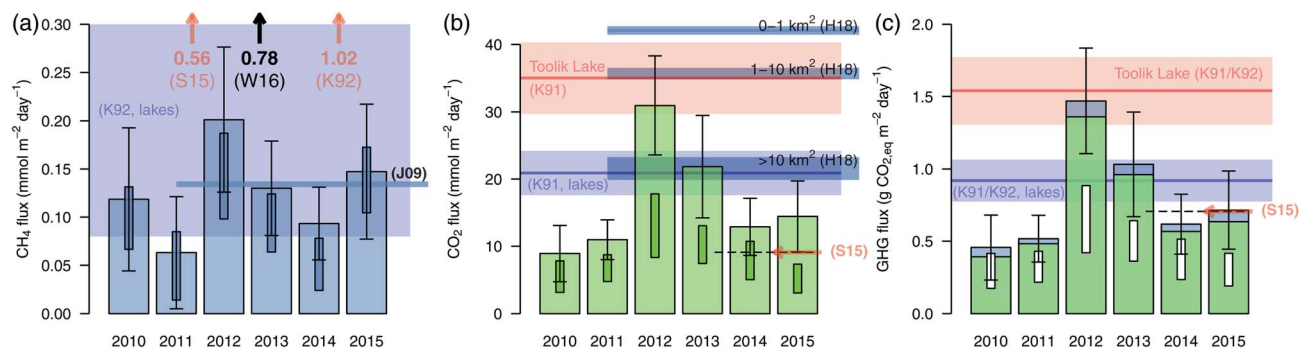

Fig. 11 Average daily fluxes of (a) CH_4, (b) CO_2, and (c) global warming potential (in CO_2-equivalents) during each ice-free periods 2010–2015 of Toolik Lake. Bars show the ice-free mean with standard deviation as vertical whiskers. The darker boxes show the inter-quartile ranges (first to third quartile) of daily medians shown in Fig. 8 and 9, and their median is shown as a white circle. The bluish and reddish bold lines (mean values) and color bands (±SD) show the ranges given by Kling *et al.* (K91)[5] for Toolik Lake (red color) and (K92)[60] for all lakes (blue color). The more recent estimates for Toolik Lake presented by Sepulveda *et al.* (S15)[61] (orange arrows; diffuse flux only, because we did not observe ebullition) and a CH_4 flux estimate by Wik *et al.* (W16)[15] (black arrow; diffuse flux only for glacial and post-glacial lakes north of 50°N) are also shown for reference. The global estimate of CH_4 fluxes of Juutinen *et al.* (J09),[74] and the CO_2 flux estimates of all boreal lakes from Hastie *et al.* (H18)[66] are shown with dark blue bars. H18 presents estimates for small (≤1 km²), middle (1–10 km²; Toolik Lake size class), and large lakes (>1 km²), which are shown separately in panel (b). An additional earlier CH_4 flux estimation is available from 14 July 1990 (red K92),[60] which is far outside the range presented in panel (a).

This journal is © The Royal Society of Chemistry 2020

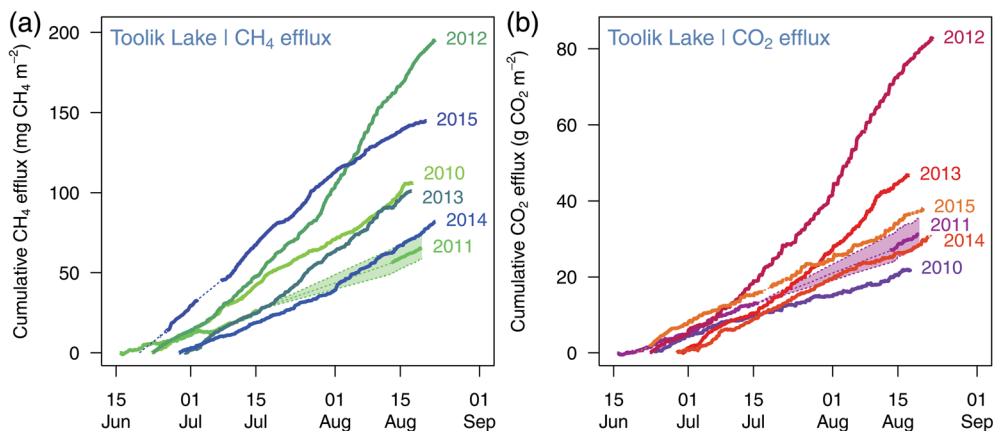*Environ. Sci.: Processes Impacts*, 2020, **22**, 2181–2198 | **2193**

Fig. 12 Cumulative fluxes of (a) CH_4 and (b) CO_2 during the ice-free periods 2010–2015 when flux instruments were active on the lake. Ice-off and refreezing were typically one to two weeks before and after instruments could be operated on the lake. A ±30% uncertainty range was added to the 2011 data due to the large data gap.

6 °C throughout the summer, which thereby limits the decomposition of organic matter in sediments in deeper locations.[64] The continuous EC measurements during multiple ice-free periods at Toolik, however, did not reveal any CH_4 emission events (detected by our 30 minute averaging period) that would suggest ebullition occurred, as has been observed elsewhere.[21] However, if ebullition is occurring frequently *via* small bubbles,

then the wavelet-based method suggested by Iwata *et al.* (2018)[65] might help to quantify the ebullition contribution after a thorough validation of the applicability of this method to lakes where ebullition is very obvious; however, this might be challenging for Toolik Lake data where ebullition is not obvious.

In the case of CO_2 flux, however, using the available data to extrapolate to summer totals might be an underestimate
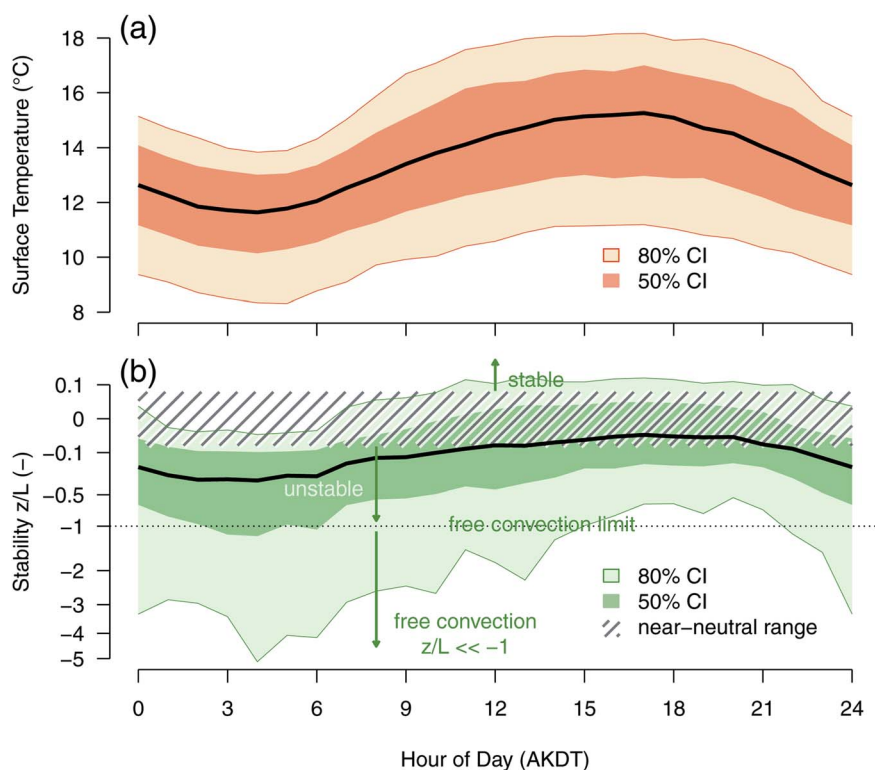

Fig. 13 Diel course of (a) lake surface temperature, and (b) atmospheric stability z/L (Monin–Obukhov stability parameter[44]). Measurements from all seasons 2010–2015 were aggregated by hour of day. The range between the 10th and 90th percentile (80% confidence interval, CI) and the inter-quartile range (50% CI) are shown with color bands, and the bold line shows the median value. Stability values in the range $-0.0625 < z/L < 0.0625$ show near-neutral stability,[75] whereas positive z/L indicate stable stratification of the atmosphere, and negative z/L unstable and convective conditions. Free convection exists if $z/L = -1$, forced convection is found under unstable conditions but with $z/L \geq -1$.

2194 | *Environ. Sci.: Processes Impacts*, 2020, **22**, 2181–2198

This journal is © The Royal Society of Chemistry 2020

because we missed the few days after removal of EC instrumentation but before the onset of ice cover (see Table 1). Within these limitations, which are the same as those of all other studies of flux measurements in the Arctic, it can be assumed that the available data provide a sound basis for estimating total gas losses from Toolik Lake, and to quantify its global warming potential during the ice-free summers.

4.5 Ice-free mean fluxes and interannual variations

Earlier estimates of CO_2 efflux from Toolik Lake (red range in Fig. 11b) and open waters globally[5,66] (blue range in Fig. 11b) provide a reference for EC fluxes measured during the 2010–2015 ice-free summers. A statistically more elaborate recent estimate by Hastie *et al.*[66] for boreal lakes of various sizes provides similar estimates for CO_2 fluxes (Fig. 11b), of which Toolik falls into the 1–10 km^2 size range. While 2012 was almost reaching earlier estimates for Toolik Lake and 2013 matched the range given for all lakes by Kling *et al.* (1991),[5] five out of six years clearly showed lower CO_2 effluxes than earlier estimates for Toolik Lake. Few CH_4 flux estimates for Toolik exist for comparison with our CH_4 results. One estimate from 1990 (ref. 60) (1.02 mmol m^{-2} d^{-1}; Fig. 11a), and a 2011–2012 estimate from another study[61] (1.25 and 0.56 mmol CH_4 m^{-2} d^{-1} for total and diffusive fluxes, respectively, assuming 100 days of ice-free conditions in summer; Fig. 11a) were much higher than what we observed with continuous EC measurements, although it should be noted that substantial differences between direct (EC) and indirect (headspace, chamber) flux measurement methods still exist. Contrastingly, the CO_2 flux estimates from the same studies were of the same order of magnitude as ours (35.0 ± 5.3 and 9.1 mmol CO_2 m^{-2} d^{-1}, respectively; Fig. 11b). These previous studies, however, were based on only one or a few measurements of the headspace equilibration method using dissolved gas concentrations combined with a surface flux model (*e.g.*, Kling *et al.*[60]) and thus lack the temporal and spatial resolution that a summer of EC measurements provides.

A comparison of the ice-free flux density estimates from 2010–2015 with similar estimates obtained from 1977–1989 (ref. 60) but with a very low number of samples ($N = 2$ to 11 per summer from 1975 to 1989, Fig. 14) shows a broad overlap of two rather different methods: (1) EC for the 2010–2015 data and (2) headspace equilibration in combination with a gradient-flux model for the 1975–1989 data.[60] Only the exceptional years 1977 and 1978 indicate much higher CO_2 effluxes than those observed in any of the EC years 2010–2015. However, in early August 2012 and 2013 the 3rd quartile of EC flux measurements of several days (Fig. 9c and d) was of the same order of magnitude as CO_2 fluxes reported from 1977 and 1978,[60] indicating that some of the earlier reported interannual variability may be an artefact of the lack of continuous observations when discrete sampling is used. In other words, the main advantage of EC flux measurements is the better temporal coverage of dynamic processes that show diel, weekly, and interannual variations as compared to random sampling with low numbers of samples.
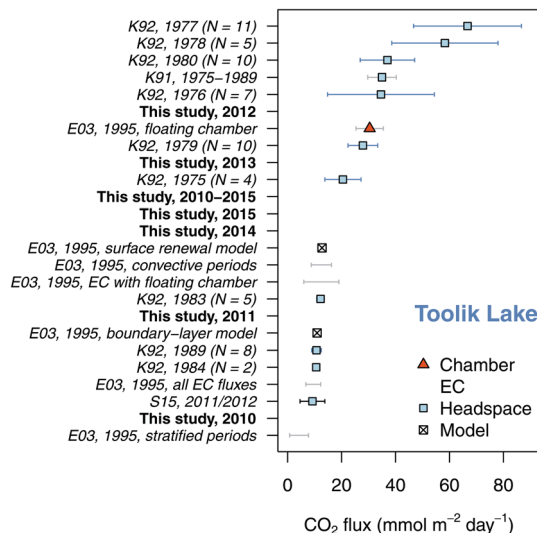

Fig. 14 Comparison of CO_2 fluxes measured during the ice-free periods 2010–2015 (bold symbols, bold font, black whiskers) with estimates from earlier publications (means ± SD): Kling *et al.* (1991; K91),[5] Kling *et al.* (1992; K92),[60] Sepulveda-Jauregui *et al.* (2015; S15),[61] and Eugster *et al.* (2003; E03).[11]

When the additional global warming potential of CH_4 fluxes from Toolik Lake are added to CO_2 flux measurements (Fig. 11c) the overall interpretation changes little as CO_2 remains the dominant climate-relevant gas flux from Toolik Lake to the atmosphere. In other words, while summer CH_4 emissions did vary annually by a factor of 4 (Fig. 11a), they were too low to rival CO_2 emissions when converted to CO_2-equivalents. Other studies in boreal and Arctic regions have found, however, that aquatic CH_4 emissions can significantly change the overall global warming potential of a system.[9,67] These studies found that CH_4 fluxes were driven by sediment temperature, depth and oxygen[67] or soil organic matter (SOM) erosion.[9] Sediment temperatures, however, remain below 5–6 °C throughout the summer, which is the typical temperature observed at the bottom of the lake. Thus, the role of lake temperature, oxygen or depth controlling the interannual variability in CH_4 flux may be limited at Toolik Lake because little change in lake temperature or oxygen has been observed from 2010 to 2015,[68] if we assume that conditions in 2010–2015 were similar to the earlier observations reported by Hobbie and Kling.[68] However, recent studies have suggested that inputs from the active layer water may be more important than internal production.[69,70]

As for SOM, Toolik Lake is a glacial lake with negligible amounts of SOM erosion observed around the lake shore (Hobbie and Kling,[68] and pers. observation), and thus the comparatively low CH_4 effluxes from Toolik would be expected. Seeing as CH_4 ebullition tends to be stochastic and higher in emission than diffusion when it does occur, its presence could cause annual variability in overall fluxes. However, we found no evidence for CH_4 ebullition *via* the sonar survey and the EC method that would capture ebullition events adequately, as in Schubert *et al.*[21] In Toolik Lake, our placement of the EC platform in 12 m of water was assumed to be representative of

average lake conditions of the >85% of the lake with depth > 2 m (see Fig. 2), and thus on the basis of a lack of clear ebullition events and a lack of CH_4 bubbles observed in the water column, we suggest that ebullition plays a negligible role in the variability of CH_4 and overall GHG effluxes at any frequency in Toolik Lake. However, potential flux peaks during the disappearance of the ice[71] or related to vernal or autumnal lake turnover[72] might be underestimated in our ice-free flux estimate in Table 1, and thus future studies should try to extend the measurements beyond the period when an EC system can safely be operated on a seasonally ice-free Arctic lake. It should also be noted that if episodic events were not detected during six years of seasonal deployment of our EC system, this does not imply that such events never occur. Our measurements represent lake depths > 2 m, and thus if such episodic events such as ebullition with much stronger fluxes should occur in the shallower areas of the lake (<2 m, 11.3% of the total lake surface; Fig. 2), then our ice-free estimates presented in Table 1 would be conservative with respect to the overall flux magnitude.

5 Conclusions

Six summers of eddy covariance CH_4 and CO_2 flux measurements on Toolik Lake indicated that earlier estimates of CO_2 efflux based on other techniques (floating chambers, gas concentration gradients) were mostly yielding the correct order of magnitude, despite the small number of samples that were taken. We found that interannual variability in gas fluxes was larger than the median diel variability of fluxes, by on average factor 4.1 for CH_4 and factor 1.8 for CO_2.

Due to lack of ebullition and the absence of large effluxes from episodic events during the ice-free periods, 86–93% of the global warming potential of Toolik Lake is due to CO_2 effluxes from the lake, with CH_4 effluxes only playing a minor role. To improve our understanding of how deep glacial lakes in the Arctic might respond to climate change, future studies should carefully investigate the drivers of the diel cycle of CH_4 and CO_2 fluxes, the trends during the ice-free period, and what drives the large interannual differences. Moreover, new approaches should be found to measure fluxes also during the critical period of ice-off and ice-on, when technical constraints limit direct measurements on the lake.

Data availability

The data used in this study can be downloaded from the Environmental Data Initiative (EDI) portal *via* DOI: 10.6073/pasta/919cd028d73ef4f8427d951148f974ec.

Conflicts of interest

The author declare no conflicts of interest.

Acknowledgements

References

1 E. A. G. Schuur, A. D. McGuire, C. Schädel, G. Grosse, J. W. Harden, D. J. Hayes, G. Hugelius, C. D. Koven, P. Kuhry, D. M. Lawrence, S. M. Natali, D. Olefeldt, V. E. Romanovsky, K. Schaefer, M. R. Turetsky, C. C. Treat and J. E. Vonk, *Nature*, 2015, **520**, 171–179.

2 Z. Tan and Q. Zhuang, *Environ. Res. Lett.*, 2015, **10**, 054016.

3 C. D. Elder, M. Schweiger, B. Lam, E. D. Crook, X. Xu, J. Walker, K. M. W. Anthony and C. I. Czimczik, *J. Geophys. Res.: Biogeosci.*, 2019, **124**, 1209–1229.

4 C. D. Elder, D. R. Thompson, A. K. Thorpe, P. Hanke, K. M. W. Anthony and C. E. Miller, *Geophys. Res. Lett.*, 2020, **47**, e2019GL085707.

5 G. W. Kling, G. W. Kipphut and M. C. Miller, *Science*, 1991, **251**, 298–301.

6 A. S. Hope, L. L. Coulter and D. A. Stow, *Int. J. Remote Sens.*, 1999, **20**, 829–835.

7 A. D. McGuire, L. G. Anderson, T. R. Christensen, S. Dallimore, L. Guo, D. J. Hayes, M. Heimann, T. D. Lorenson, R. W. Macdonald and N. Roulet, *Ecol. Monogr.*, 2009, **79**, 523–555.

8 B. Riordan, D. Verbyla and A. D. McGuire, *J. Geophys. Res.: Biogeosci.*, 2006, **111**, G04002.

9 K. Walter Anthony, R. Daanen, P. Anthony, T. S. von Deimling, C.-L. Ping, J. P. Chanton and G. Grosse, *Nat. Geosci.*, 2016, **9**, 679–682.

10 G. Myhre, D. Shindell, F.-M. Bréon, W. Collins, J. Fuglestvedt, J. Huang, D. Koch, J.-F. Lamarque, D. Lee, B. Mendoza, T. Nakajima, A. Robock, G. Stephens, T. Takemura and H. Zhang, in *Climate Change 2013: The Physical Science Basis. Contribution of Working Group I to the Fifth Assessment Report of the Intergovernmental Panel on Climate Change*, ed. T. F. Stocker, D. Qin, G.-K. Plattner, M. Tignor, S. K. Allen, J. Boschung, A. Nauels, Y. Xia, V. Bex and P. M. Midgley, Cambridge University Press, Cambridge, United Kingdom and New York, NY, USA, 2013, ch. Anthropogenic and Natural Radiative Forcing, pp. 129–234.

11 W. Eugster, G. Kling, T. Jonas, J. P. McFadden, A. Wüest, S. MacIntyre and F. S. Chapin III, *J. Geophys. Res.*, 2003, **108**, 4362–4380.

12 K. M. Walter, S. A. Zimov, J. P. Chanton, D. Verbyla and F. S. Chapin III, *Nature*, 2006, **443**, 71–75.

13 T. R. Christensen, *Nature*, 2014, **509**, 279–281.

14 M. Jammet, P. Crill, S. Dengel and T. Friborg, *J. Geophys. Res.: Biogeosci.*, 2015, **120**, 2289–2305.

2196 | *Environ. Sci.: Processes Impacts*, 2020, **22**, 2181–2198

This journal is © The Royal Society of Chemistry 2020

15 M. Wik, R. K. Varner, K. W. Anthony, S. MacIntyre and D. Bastviken, *Nat. Geosci.*, 2016, **9**, 99–105.

16 A. Townsend-Small, F. Åkerström, C. D. Arp and K. M. Hinkel, *J. Geophys. Res.: Biogeosci.*, 2017, **122**, 2966–2981.

17 M. A. Holgerson and P. A. Raymond, *Nat. Geosci.*, 2016, **9**, 222–226.

18 C. D. Elder, X. Xu, J. Walker, J. L. Schnell, K. M. Hinkel, A. Townsend-Small, C. D. Arp, J. W. Pohlman, B. V. Gaglioti and C. I. Czimczik, *Nat. Clim. Change*, 2018, **8**, 166–171.

19 M. Wik, B. F. Thornton, D. Bastviken, J. Uhlbäck and P. M. Crill, *Geophys. Res. Lett.*, 2016, **43**, 1256–1262.

20 E. Podgrajsek, E. Sahlée, D. Bastviken, J. Holst, A. Lindroth, L. Tranvik and A. Rutgersson, *Biogeosciences*, 2014, **11**, 4225–4233.

21 C. J. Schubert, T. Diem and W. Eugster, *Environ. Sci. Technol.*, 2012, **46**, 4515–4522.

22 S. Sollberger, B. Wehrli, C. J. Schubert, T. DelSontro and W. Eugster, *Environ. Sci.: Processes Impacts*, 2017, **19**, 1278–1291.

23 D. Bastviken, A. L. Santoro, H. Marotta, L. Q. Pinho, D. F. Calheiros, P. Crill and A. Enrich-Prast, *Environ. Sci. Technol.*, 2010, **44**, 5450–5455.

24 P. M. Crill, K. B. Bartlett, J. O. Wilson, D. I. Sebacher, R. C. Harriss, J. M. Melack, S. MacIntyre, L. Lesack and L. Smith-Morrill, *J. Geophys. Res.*, 1988, **93**, 1564.

25 K.-M. Erkkilä, A. Ojala, D. Bastviken, T. Biermann, J. J. Heiskanen, A. Lindroth, O. Peltola, M. Rantakari, T. Vesala and I. Mammarella, *Biogeosciences*, 2018, **15**, 429–445.

26 J. Jansen, B. F. Thornton, A. Cortés, J. Snöälv, M. Wik, S. MacIntyre and P. M. Crill, *Biogeosciences*, 2020, **17**, 1911–1932.

27 A. Cortés, S. MacIntyre and S. Sadro, *Limnol. Oceanogr.*, 2017, **62**, 2023–2044.

28 W. Eugster and P. Plüss, *Agric. For. Meteorol.*, 2010, **150**, 841–851.

29 T. Vesala, W. Eugster and A. Ojala, in *Eddy covariance measurements over lakes*, ed. M. Aubinet, T. Vesala and D. Papale, Springer, Dordrecht Heidelberg London New York, 2012, ch. 15, pp. 365–376.

30 M. Mauder, T. Foken, R. Clement, J. A. Elbers, W. Eugster, T. Grünwald, B. Heusinkveld and O. Kolle, *Biogeosciences*, 2008, **5**, 451–462.

31 *Eddy Covariance – A Practical Guide to Measurement and Data Analysis*, ed. M. Aubinet, T. Vesala and D. Papale, Springer, Dordrecht Heidelberg London New York, 2012.

32 C. Rebmann, O. Kolle, B. Heinesch, R. Queck, A. Ibrom and M. Aubinet, in *Data Acquisition and Flux Calculations*, ed. M. Aubinet, T. Vesala and D. Papale, Springer, Dordrecht Heidelberg London New York, 2012, ch. 3, pp. 59–84.

33 T. Foken, R. Leuning, S. R. Oncley, M. Mauder and M. Aubinet, in *Corrections and data quality control*, ed. M. Aubinet, T. Vesala and D. Papale, Springer, Dordrecht Heidelberg London New York, 2012, ch. 4, pp. 85–131.

34 E. K. Webb, *Bound.-Layer Meteorol.*, 1982, **23**, 251–254.

35 R. V. Hiller, C. Zellweger, A. Knohl and W. Eugster, *Atmos. Meas. Tech. Discuss.*, 2012, **5**, 351–384.

36 F. G. Wienhold, H. Fischer and G. W. Harris, *Infrared Phys. Technol.*, 1996, **37**, 67–74.

37 W. Eugster, *Proceedings of the Fourth International Conference on Fog, Fog Collection and Dew*, La Serena, Chile, 2007, pp. 359–362.

38 W. Eugster and L. Merbold, *Soil*, 2015, **1**, 187–205.

39 S. Osterwalder, W. Eugster, I. Feigenwinter and M. Jiskra, *Atmos. Meas. Tech.*, 2020, **13**, 2057–2074.

40 T. Foken, M. Göckede, M. Mauder, L. Mahrt, B. Amiro and W. Munger, in *Post-field data quality control*, ed. X. Lee, W. Massman and B. Law, Kluwer, Dordrecht, 2004, ch. 9, pp. 181–208.

41 C. Schaller, F. Kittler, T. Foken and M. Göckede, *Atmos. Chem. Phys.*, 2019, **19**, 4041–4059.

42 R. B. Stull, *An Introduction to Boundary Layer Meteorology*, Kluwer, Dordrecht, 1988.

43 S. P. S. Arya, *Introduction to Micrometeorology*, Academic Press, San Diego, 1988.

44 A. S. Monin and A. M. Obukhov, *Tr. Geofiz. Inst., Akad. Nauk SSSR*, 1954, **24**, 163–187.

45 R Core Team, *R: A Language and Environment for Statistical Computing*, R Foundation for Statistical Computing, Vienna, Austria, 2019.

46 G. P. Nason, *Wavelet Methods in Statistics with R*, Springer, New York, 2008.

47 J. Morlet, G. Arens, E. Fourgeau and D. Giard, *Geophysics*, 1982, **47**, 203–221.

48 N. Kljun, P. Calanca, M. W. Rotach and H. P. Schmid, *Bound.-Layer Meteorol.*, 2004, **112**, 503–523.

49 N. Kljun, P. Calanca, M. W. Rotach and H. P. Schmid, *Geosci. Model Dev.*, 2015, **8**, 3695–3713.

50 L. C. Loken, J. T. Crawford, P. J. Schramm, P. Stadler, A. R. Desai and E. H. Stanley, *J. Geophys. Res.: Biogeosci.*, 2019, **124**, 2248–2266.

51 T. DelSontro, D. F. McGinnis, B. Wehrli and I. Ostrovsky, *Environ. Sci. Technol.*, 2015, **49**, 1268–1276.

52 W. Eugster and M. J. Zeeman, *Int. Congr. Ser.*, 2006, **1293**, 66–75.

53 T. DelSontro, M. J. Kunz, T. Kempter, A. Wüest, B. Wehrli and D. B. Senn, *Environ. Sci. Technol.*, 2011, **45**, 9866–9873.

54 J. J. Finnigan, R. Clement, Y. Malhi, R. Leuning and H. A. Cleugh, *Bound.-Layer Meteorol.*, 2003, **107**, 1–48.

55 J. Moncrieff, R. Clement, J. Finnigan and T. Meyers, in *Averaging, detrending, and filtering of eddy covariance time series*, ed. X. Lee, W. Massman and B. Law, Kluwer, 2004, ch. 2, pp. 7–31.

56 E. Podgrajsek, E. Sahlée and A. Rutgersson, *J. Geophys. Res.: Biogeosci.*, 2014, **119**, 236–248.

57 E. Podgrajsek, E. Sahlée and A. Rutgersson, *J. Geophys. Res.: Biogeosci.*, 2015, **120**, 29–38.

58 T. Vesala, J. Huotari, Ü. Rannik, T. Suni, S. Smolander, A. Sogachev, S. Launiainen and A. Ojala, *J. Geophys. Res.: Atmos.*, 2006, **111**, D11101.

This journal is © The Royal Society of Chemistry 2020

Environ. Sci.: Processes Impacts, 2020, **22**, 2181–2198 | 2197

59 J. J. Heiskanen, I. Mammarella, S. Haapanala, J. Pumpanen, T. Vesala, S. MacIntyre and A. Ojala, *Tellus B*, 2014, **66**, 22827.

60 G. W. Kling, G. W. Kipphut and M. C. Miller, *Hydrobiologia*, 1992, **240**, 23–36.

61 A. Sepulveda-Jauregui, K. M. W. Anthony, K. Martinez-Cruz, S. Greene and F. Thalasso, *Biogeosciences*, 2015, **12**, 3197–3223.

62 K. M. W. Anthony, D. A. Vas, L. Brosius, F. S. Chapin, S. A. Zimov and Q. Zhuang, *Limnol. Oceanogr.: Methods*, 2010, **8**, 592–609.

63 R. C. H. Aben, N. Barros, E. van Donk, T. Frenken, S. Hilt, G. Kazanjian, L. P. M. Lamers, E. T. H. M. Peeters, J. G. M. Roelofs, L. N. de Senerpont Domis, S. Stephan, M. Velthuis, D. B. V. de Waal, M. Wik, B. F. Thornton, J. Wilkinson, T. DelSontro and S. Kosten, *Nat. Commun.*, 2017, **8**, 1682.

64 C. Gudasz, D. Bastviken, K. Steger, K. Premke, S. Sobek and L. J. Tranvik, *Nature*, 2010, **466**, 478–481.

65 H. Iwata, R. Hirata, Y. Takahashi, Y. Miyabara, M. Itoh and K. Iizuka, *Bound.-Layer Meteorol.*, 2018, **169**, 413–428.

66 A. Hastie, R. Lauerwald, G. Weyhenmeyer, S. Sobek, C. Verpoorter and P. Regnier, *Glob. Change Biol.*, 2018, **24**, 711–728.

67 E.-I. Rõõm, P. Nõges, T. Feldmann, L. Tuvikene, A. Kisand, H. Teearu and T. Nõges, *J. Hydrol.*, 2014, **519**, 1594–1606.

68 *Alaska's Changing Arctic: Ecological Consequences for Tundra, Streams, and Lakes*, ed. J. E. Hobbie and G. W. Kling, Oxford University Press, New York, USA, 2014.

69 A. L. Lecher, P.-C. Chuang, M. Singleton and A. Paytan, *J. Geophys. Res.: Biogeosci.*, 2017, **122**, 753–766.

70 A. Paytan, A. L. Lecher, N. Dimova, K. J. Sparrow, F. G.-T. Kodovskac, J. Murraya, S. Tulaczyka and J. D. Kessler, *Proc. Natl. Acad. Sci. U. S. A.*, 2015, **112**, 3636–3640.

71 B. A. Denfeld, H. M. Baulch, P. A. del Giorgio, S. E. Hampton and J. Karlsson, *Limnol. Oceanogr. Lett.*, 2018, **3**, 117–131.

72 J. López Bellido, T. Tulonen, P. Kankaala and A. Ojala, *J. Geophys. Res.*, 2009, **114**, G04007.

73 Toolik EDC, *Annual Summaries from the Naturalist Journal*, Environmental Data Center, 2020, https://toolik.alaska.edu/edc/journal/annual.php, last accessed 2020-05-06.

74 S. Juutinen, M. Rantakari, P. Kortelainen, J. T. Huttunen, T. Larmola, J. Alm, J. Silvola and P. J. Martikainen, *Biogeosciences*, 2009, **6**, 209–223.

75 T. Foken and B. Wichura, *Agric. For. Meteorol.*, 1996, **78**, 83–105.